Investigation of array layout of tidal stream turbines on energy extraction efficiency

Can Zhang[1,2], Jisheng Zhang[1,2], Linlong Tong[1,2], Yakun Guo[2,3], Peng Zhang[4]

[1] Key Laboratory of Coastal Disaster and Defence (Hohai University), Ministry of Education, China

[2] College of Harbor, Coastal and Offshore Engineering, Hohai University, Nanjing, 210098, China

[3] Faculty of Engineering & Informatics, University of Bradford, Bradford, BD7 1DP, UK

[4] China Three Gorges Corporation, Beijing, 100038, China

Corresponding email: y.guo16@bradford.ac.uk

ABSTRACT

A two-dimensional model based on OpenTidalFarm is applied to simulate tidal stream flow around turbines. The model is governed by shallow water equations and is able to optimize the layout of the deployed turbine array in terms of maximizing the energy outputs. Three turbine array layouts including two structured layouts (regular and staggered) and one unstructured layout (optimized) are simulated to investigate the effect of turbine layouts on energy extraction. The present study shows that more energy could be extracted when lateral spacing decreases and longitudinal spacing increases within the same domain, namely the effective turbine layout is to deploy more turbines in the first row to extract energy from undisturbed tidal stream, while larger longitudinal spacing will make it possible for tidal stream to recover more before reaching the next turbines row. Taking the tidal stream turbines array around Zhoushan Islands as a case study, results show that the optimized layout can extract 106.8% energy of that extracted by the regular and staggered layout for a full tide in the same marine area. Additionally, the turbine array has a great influence on tidal stream velocities immediately behind the array and has little effect on far-field wake flow.

Keywords: turbine array layout; tidal stream energy; shallow water equations; Zhoushan Islands.

1. Introduction

With the increasing attentions to the environmental issue, fossil fuels which are unfriendly to the environment and have limited storage will generally be replaced by renewable energy. Though offshore wind farms have been substantially built around the world (Lin, et al. 2017), tidal stream energy is becoming more and more popular, partly due to its predictable feature (Zhang et al., 2013). The potential tidal stream energy around the Zhoushan Islands, China, is abundant. The maximum tidal stream velocity in the channel between the Hulu Island and Putuoshan Island is above 1.7 m/s with water depth varying between 20 m to 60 m (Wang et al., 2010). As a result, the first million watt (MW) size tidal stream energy demonstrative project of China is located here. In this paper, different turbine array layouts are compared in order to seek for the most suitable one.

To effectively extract the tidal stream energy, tidal stream turbines must be deployed in the form of array in the field. This raises questions about how to deploy the turbines in an array to maximize the energy output and to minimize the environment impacts caused by the deployment of tidal turbines array. There is a huge difference between deploying one turbine and deploying one array comprising of tens of turbines (Vennell et al., 2015). Once the type of a turbine is fixed, the turbine can be maximized in terms of its energy output by deploying at the point where the tidal stream velocity is the maximum. However, as one array may contain tens of turbines, the interaction between these turbines cannot be neglected (Odohert et al., 2011). In other words, the maximum energy output cannot be achieved by just deploying the whole array at the area in which the tidal stream velocity is high, because the spacing between these turbines should also be considered.

Extensive studies have been carried out to investigate the recovery of the tidal stream velocity in the wake of a single turbine in order to examine the optimum spacing between two turbines for maximizing the tidal stream energy outputs (Zhang et al., 2017; Xin et al., 2011; Chen, 2015; An, 2012; Malki et al., 2013). These studies found that the tidal stream velocity could recover up to 80% about 20*D* (*D* is the diameter of the turbine) downstream of the turbine and 100% tidal stream velocity could recover at 40*D* downstream of the turbine. As the turbine can be significantly affected by the turbines around it (Mycek et al., 2012), both the longitudinal spacing and the lateral spacing between the turbines in an array have effect on the tidal stream velocity recovery. Odoherty et al. (2011) studied the interaction between closely deployed turbines by simulating a small array of turbines. They found that the optimum of turbine array in terms of the efficiency of extracting tidal stream energy was achieved when the lateral spacing was about 2*D* and streamwise spacing was around 5*D*. When the second row was staggered, it could extract 80% energy of that of the first row.

By simplifying the tidal stream model, the turbine array layouts can be investigated analytically. An optimized simple model was used by Garrett and Cummins (2008) to estimate the maximum energy that could be extracted from the tidal stream along a channel. Vennell (2010, 2011) applied one-dimensional models to investigate the effect of tuning each turbine in the array to consider the effect of the channel geometry, turbine position and the tidal forcing on the turbine array energy extraction efficiency. However, these simple models could not simulate the complex interaction between the turbines, which is important for tidal stream energy extraction (Funke et al., 2014).

Many mathematical optimization strategies and models have also been proposed to optimize

the layout of turbine array. The gradient-based optimization method was developed to improve the layout in which the energy output was considered to be the function of interest (Funke et al., 2014, 2016). González-Gorbeña et al. (2016, 2018) applied a surrogate-based optimization of computational fluid dynamic experiments to optimize the uniform turbine array layout. However, to the best of authors' knowledge, little explanation was given for the optimized turbine array layout about why they extracted more energy. Furthermore, few studies have been conducted to compare the impacts on environment caused by different turbine array layouts.

In this paper, a numerical model based on OpenTidalFarm (OpenTidalFarm 2014) is used to investigate the tidal stream around Zhoushan Islands, China, and the impacts that may be caused by different turbine array layouts. As the turbine array layout optimized by OpenTidalFarm is unstructured, which is novel comparing to the structured layouts; it is important to investigate the physical mechanism of this new layout type and its advantages and disadvantages. To this end, a turbine array consisting of 18 turbines is used and arranged in three layouts in order not only to compare the energy extraction efficiency, but also to analyze their wake characteristics. It is expected that this study will provide some adequate advice for deployment of tidal stream turbines around Zhoushan Islands in terms of maximum exploiting tidal stream energy.

2. Numerical model

The numerical simulation is carried out using the OpenTidalFarm, which is an open-source software and has the capability of flow prediction and efficient tidal turbine layout optimization. OpenTidalFarm was recently developed for improving the energy extracting ability of the layout (Funke et al., 2014) and seeking for the maximum number of turbines in a given deployment area (Funke et al., 2016). It was further developed to consider the cost of

deployment (Cully et al., 2016) and the size of the arrays with a surrogate-model (Cully et al., 2017) as well as the trade-off between energy yield and impact on flow (Feu et al., 2017). Although OpenTidalFarm has some limitations: (1) the ignorance of the turbine's blades and the support structure may lead to certain errors in simulating tidal current; and (2) the initial layout can affect the final optimization as the optimization algorithm can only just find a local optimal result, it can provide the appropriate and effective turbine array layout with acceptable error.

2.1 Treatment of turbine array

In this study, the two-dimensional (2D) hydrodynamic model based on OpenTidalFarm is used to simulate the tidal stream around the Zhoushan Islands. The initial structured turbine array layout is optimized by using the sequential quadratic programming, which is considered to be one of the most efficient optimization algorithms (Boggs and Tolle, 1995).

The turbine is modelled as a bottom friction in a square area whose side length is the same as the turbine's diameter. This bottom friction coefficient increases from zero at the side to a given value K_i at the center (Divett et al., 2013). Therefore, for the i th turbine, it can be parameterized as:

$$C_i = K_i \psi_{x_i,y_i,r}, \tag{1}$$

$$\psi_{p,r}(x) = \begin{cases} e^{1-1/\left(1-\left\|\frac{x-p}{r}\right\|^2\right)} & \text{for } \left\|\frac{x-p}{r}\right\|, \\ 0 & \text{otherwise,} \end{cases} \tag{2}$$

where C_i is the friction of the i th turbine, K_i is a friction coefficient centered at the point (x_i, y_i), $\psi_{x_i,y_i,r}$ is a two-dimensional bump function obtained by multiplying equation (2) in both independent dimensions, p is the center point's coordinate of the bump function, r is the radius of the turbine.

A turbine array consisting of many turbines can be parameterized as:

$$c_t(\boldsymbol{m}) = \sum_{i=1}^{N} C_i, \tag{3}$$

where $c_t(\boldsymbol{m})$ is the total friction of all the turbines, N is the number of the turbines, **m** is a 2n-long vector which contains the coordinates of all the turbines.

2.2 Governing equations

In this model, the governing equations are the 2D shallow water equations:

$$\kappa\frac{\partial u}{\partial t} + u \cdot \nabla u - \upsilon\nabla^2 u + g\nabla\eta + \frac{c_b + c_t(\boldsymbol{m})}{H}\|u\|u = 0, \tag{4}$$

$$\kappa\frac{\partial \eta}{\partial t} + \nabla \cdot (Hu) = 0, \tag{5}$$

where κ is the parameter which specifies whether the problem is stationary ($\kappa = 0$) or non-stationary ($\kappa = 1$), u is the depth-averaged velocity in m/s, η is the free-surface displacement in m, H is the water depth at rest in m, g is gravitational acceleration in m/s^2, υ is the viscosity coefficient in m^2/s, c_b is the bottom friction in Newton.

These equations are discretized with the finite element method. The weak form is derived by multiplying the shallow water equations with test functions, integrating over the computational domain and applying integration by parts to select terms. For the velocity and the free-surface displacement, piecewise quadratic functions and piecewise linear functions are used respectively on each triangle over the suitable triangulation of the computational domain. In terms of the time discretization, the implicit Euler method is used because of its unconditional stability and simplicity.

2.3 Initial and boundary conditions

2.3.1 Initial conditions

The initial conditions are controlled by following equations:

$$u_x(x,y,t)|t = t_0 = u_{x0}(x,y,t_0) \quad (6a)$$

$$u_y(x,y,t)|t = t_0 = u_{y0}(x,y,t_0) \quad (6b)$$

$$\eta(x,y,t)|t = t_0 = \eta_0(x,y,t_0) \quad (6c)$$

where $u_{x0}(x,y,t_0)$ and $u_{y0}(x,y,t_0)$ is respectively the velocity component in *x* and *y* direction at initial time t_0, $\eta_0(x,y,t_0)$ is the tidal height at initial time t_0. In this study, they are all set as zero.

2.3.2 Boundary conditions

A Dirichlet boundary condition is applied to specify the velocity at the inlet boundary. The free-surface displacement of the outflow boundary is set to zero. On the boundaries of the island and inland, the normal component of the velocity is set to zero; while for the tangential component a free-slip condition is imposed. The tidal condition is determined by combining the eight main tidal constituents, namely Q1, U1, P1, K1, N2, M2, S2, and K2, which are provided by the global tidal model TPX08-atlas (Zhang et al., 2018).

2.4 Optimization model

The model developed by Funke et al. (2014) which optimizes the turbine array layout to maximize the energy extraction is used in this study:

$$\begin{aligned} \max \quad & \mathrm{J}(\mathrm{z}, \boldsymbol{m}) \\ \text{subject to} \quad & \mathrm{F}(\mathrm{z}, \boldsymbol{m}) = 0, \\ & b_l \leq m \leq b_u, \\ & \mathrm{g}(\boldsymbol{m}) \leq 0, \end{aligned} \quad (7)$$

where $\mathrm{J}(\mathrm{z}, \mathbf{m})$ is the function of interest, $\mathrm{F}(\mathrm{z}, \boldsymbol{m})$ is a partial differential equations (PDE) operator containing the shallow water equations (equation 4 and equation 5), $\mathrm{z} = (u, \eta)$ is the solution of the shallow water equations, b_l and b_u are the bounds of the area where turbines are deployed, $\mathrm{g}(\boldsymbol{m})$ is used to keep the spacing between two turbines beyond the minimum distance.

In this model, the coordinates of each turbine $\boldsymbol{m}$ are treated as the control parameters. The time-averaged energy extracted by turbine array, which is also the function of interest (Sutherland et al., 2007; Vennell, 2012; Funke et al., 2014), is calculated as:

For $\kappa = 1$:

$$\mathrm{P}(\boldsymbol{m}) = \frac{1}{T}\int_0^T \int_\Omega \rho\, c_t(\boldsymbol{m}) \|u\|^3 dx \tag{8}$$

For $\kappa = 0$:

$$\mathrm{P}(\boldsymbol{m}) = \int_\Omega \rho\, c_t(\boldsymbol{m}) \|u\|^3 dx \tag{9}$$

Equation (8) is for non-stationary ($\kappa = 1$) and equation (9) is for stationary ($\kappa = 0$). At each optimization iteration, the coordinates of each turbine are updated to improve the extraction of more energy, $\mathrm{P}(\boldsymbol{m})$.

2.5 Description of the study area

The Zhoushan Islands are situated in Zhejiang Province, China. The channel, as shown in Figure 1, is between the Hulu Island and Putuoshan Island and is chosen as the study area to deploy the turbines. In order to avoid the influence from the boundary effect, in this model, the computational domain is much larger than the study area, which varies from 122.295° to 122.568° at east longitude and from 29.848° to 30.160° at north latitude. Both the Hulu Island and the Putuoshan Island, which belong to the Zhoushan Islands, are included. The mesh element

used in this model is unstructured triangle, which allows the flexible assignment and refine in the concerned regions of meshes (Guo et al. 2012, 2014). The resolution of the mesh varies from 500m at the model boundaries to 2m near the study channel. The final meshes have 39002 nodes and 79788 triangle elements, as shown in Figure 2. The roughness coefficient is considered to be constant and set as 0.0025 (Wang, 2018). The eddy viscosity coefficient is taken as 10 m^2/s. To ensure numerical stability, the boundaries viscosity coefficient is set to be 100 m^2/s and the computational time step is set to be 30 s.

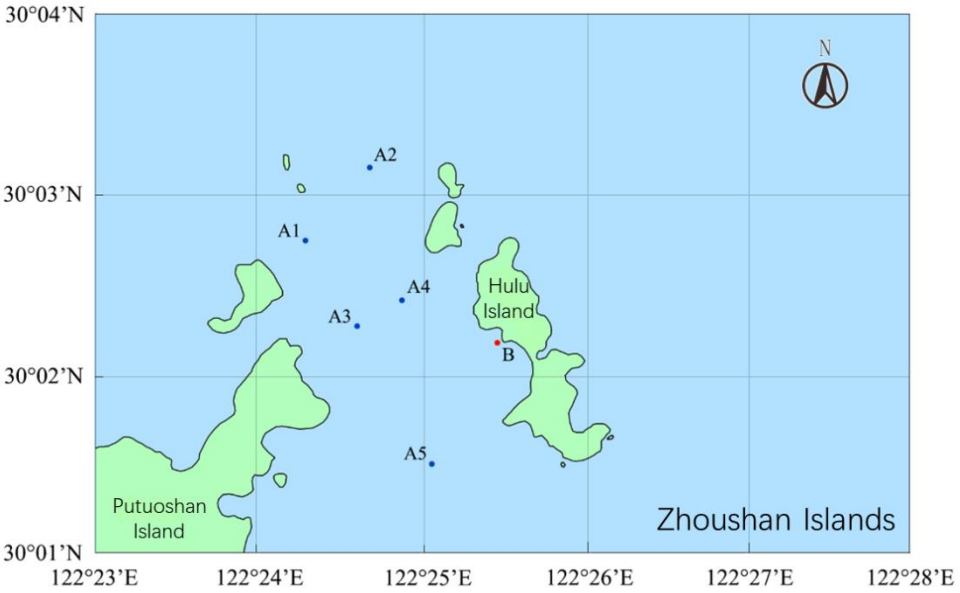

Figure 1. Positions of the five tidal stream stations and the tidal height station (adopted from Wang, 2018)

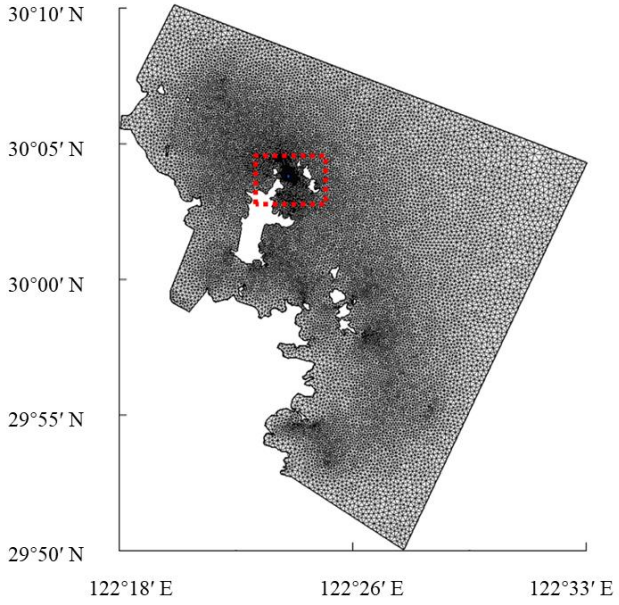

Figure 2. Computational domain of Zhoushan Islands with the study channel inside the red dosh rectangle.

3. Results and discussion

3.1 Model validation

3.1.1 Tidal stream model validation

To evaluate the model capability on simulating tidal stream, field observed data of the tidal heights and tidal stream velocities are used to validate the model. These data are gained from the demonstrative project of tidal stream energy in Zhoushan Island, Zhejiang province. The measured tidal heights data are from 12 August to 27 August 2013 at station B (see Figure 1). The measured tidal stream velocities data including the neap tides, the middle tides and the spring tides are collected from 16 August to 24 August 2013.

Figure 3 is the comparison of simulated (solid line) and measured (open circles) tidal elevations. It is seen from Figure 3 that the simulated tidal heights agree well with the measurements. Some deviation between the simulation and measurement is seen to take place during the spring tide. The relative maximum error, calculated as the ratio of the difference between the measured and simulated tidal heights over the measured local tidal range, is about 10%, which meets the UK model

validation criteria (15% of the spring tidal range) (Evans 1993; Zhang et al. 2019).

Figure 4 is the comparison between simulated (solid lines) and measured (open circles) tidal stream velocity (a) and tidal stream direction (b) at tide monitoring station A5. Figure 4 shows that in general, the simulated tidal flow direction agrees well with the measurements. The largest error takes place at the neap tide. Figure 4(a) demonstrates that the simulated velocity magnitude favorably agrees with the measured velocity magnitude though some discrepancy between simulation and observation exists with the relative maximum error (~45%) taking place at 21pm 16 August. The reasons for this large simulation error are: (1) the computational mesh nodes from which the velocity is outputted, may not exactly coincide with the tide observation monitoring stations; which will generate some error; (2) due to the limitation of the field data, the seabed roughness coefficient is considered as constant for the whole computational domain, which may not be the real situation; and (3) the model didn't consider the effect of wind on the sea surface for simplification. On the other hand, some error may come from the field measurements, which were carried out in the harsh and difficult control marine environment.

In addition to analysis of relative error, the statistical errors, namely the mean absolute error (MAE) and the root mean square error (RMSE) between the simulated and observed data are also calculated and listed in Table 1. Generally speaking, the model can be considered to have the capability of predicting the tidal stream around Zhoushan Islands with reasonable accuracy.

3.1.2 Turbine model validation

The turbine model validation was carried out by the authors who conducted laboratory experiments to investigate the wake characteristics of a horizontal tidal turbine (Zhang et al.

2020).In the laboratory experiment the three-bladed horizontal tidal stream turbine with 27cm in diameter was put in a re-circulation flume, which has a working section of 50 m in length, 1.2 m in width and 1.2 m in depth. The numerical model with the same size is run in the OpenTidalFarm. Figure 5 shows the comparison of the simulated (solid lines) and the measured velocity profiles (open circles).

In general, Figure 5 shows that the simulated velocity in the wake region agrees well with the measurements. It is noticeable that the recover tendency of the velocity in the wake area is well simulated especially for the minimum velocity in each cross section. Some errors are seen to appear in the near wake area, e.g.1D, 2D behind the turbine. This deviation is perhaps ascribed to the fact that the turbine blades and the support structure are ignored in the simulation.

3.2 Sensitivity analysis of mesh size on computational results

The reliability and accuracy of simulation results of numerical models are normally evaluated through mesh size sensitivity analysis. In this study, four mesh sizes, as listed in Table 2, are designed to investigate the mesh dependency, ranging from 4310 nodes and 8964 cells (mesh 4) to 130280 nodes and 263747 cells (mesh 1) in the computational domain. As this study focuses on simulating the velocity field, only the accuracy of the simulated velocity is compared with the measurements. Figure 6 shows the comparison the simulated (solid lines) and field observed (open circles) velocity for various mesh sizes. Figure 6 demonstrates that there is a relatively large difference between the simulated and observed velocity for very coarse mesh (e.g. mesh 4: 4310 nodes and 8964 cells). The simulation is greatly improved when the mesh density increases from 4310 nodes and 8964 cells to 39002 nodes and 79788 cells (mesh 2). Using the same analysis

method mentioned by Chen et al. (2013); the maximum mean absolute error (MAE) and the maximum root mean square error (RMSE) between the simulated and measured velocity are both improved from 0.1215 to 0.0918 and from 0.1250 to 0.1125, respectively. When the mesh is continuously refined from mesh 2 to mesh 1, no noticeable improvement is achieved, while the computational time increases a magnitude of an order. Therefore, considering the computational efficiency and accuracy, the finalized mesh used in this study has 39002 nodes and 79788 cells (mesh 2). This mesh configuration enables the model to provide tidal velocity with sufficient accuracy, which is of significance in terms of evaluating the potential tidal stream energy.

3.3 Turbine array layout description

The validated model is applied to evaluate the tidal stream energy around Zhoushan Islands in which 18 turbines with the same diameter of 20 m are planned to deploy. As the type of the turbine is not main topic in this study, the friction coefficients of all turbines are set as the default value, i.e. 12. The minimum spacing between two turbines is set as 30m. The simulation starts at 8:30am, 22 August 2013 and runs for 35h to include a 12h full tide (from 5:30am, 23 August 2013 to 17:30pm, 23 August 2013). The computational time step is set as 30min.

For the structured regular layout, the turbines are deployed in a way that the lateral spacing is 2D and the vertical spacing is 5D, as shown in Figure 7(a). For the structured staggered layout, the spacing is the same as that with structured regular layout (see Figure 7(b)) with the turbines in the even row being deployed at the gap between the turbines in the odd row. This staggered layout is expected to be the most effective structured layout in terms of extracting tidal stream energy (Odeherty et al., 2011). For the optimized layout, the turbines are deployed in an unstructured pattern

which looks like a barrage with three layers, as shown in Figure 8. Each row is perpendicular to the flowing direction for all three layouts.

3.4 Energy extraction

Figure 9 shows the power extraction by three turbine layouts over twelve hours. As the extracted power is proportional to the cube of the velocity, the power extraction by these three turbine layouts vary mainly with the tidal stream velocity. When the velocity at the target area reaches the peak (e.g. 9:30am), the gap between ability to extract tidal stream energy by these three layouts is likely to widen. Integrating the power over time in Figure 9 yields the energy extracted by the structured regular layout and staggered layout during 12h being 6.15×10^4 kW·h and 6.24×10^4 kW·h respectively and 6.56×10^4 kW·h for the optimized layout. The optimized layout has been achieved after 47 times simulations until the improvements of the energy outputs from the last layout to the immediate previous layout is less than 0.1% (shown in Figure 8). Comparing the normal staggered layout with 2D lateral spacing and 5D vertical spacing and the optimized staggered layout, the latter can extract 5% more tidal stream energy than the former, showing a great energy extraction efficiency. This demonstrates that higher energy extraction could be achieved when the tidal turbine layout is deployed in an unrestricted way, which is interpreted as follows.

As shown in Figure 10 (a), the first row turbines in structured regular layout can extract the energy from undisturbed tidal stream, indicating that these turbines are fully utilized. The other turbine rows behind the first row are deployed in the tidal stream velocity deceleration area and thus, the energy extracted by these turbines is less.

The structured staggered layout, as shown in Figure 10(b), is similar to that in Figure 10(a). However, as the odd rows interlace with the even row, turbines in the downstream row are able to extract energy from the locally accelerated tidal stream due to the narrowing effect of the front row. This makes the structured staggered layout extract more energy than that the structured regular layout does.

For the optimized layout showed in Figure 10(c), the turbine array is deployed in 3 rows. Three turbines are placed in the first row, which extract energy from undisturbed tidal stream. In the second row, four turbines are divided into two parts with three turbines being placed on the west and one turbine on the east. These turbines are deployed in the local tidal flow accelerating area behind the first row, enabling these turbines to extract more energy. The third row has eleven turbines and is placed behind the first row. Though tidal stream velocity downstream of the first row is reduced due to some tidal stream energy extracted, the large spacing between the first and third rows makes it possible that the tidal stream velocity recovers to a high level. Furthermore, blockage induced by the second row may increase the tidal stream velocity downstream. These make the eleven turbines in the third row to extract more tidal stream energy. As a result, the unstructured optimized layout extracts more energy than the other two structured layouts.

The above analysis demonstrates that to increase the tidal stream energy extraction, turbines should be placed in the area where the tidal stream velocity is not significantly decelerated or the tidal flow is locally accelerated. This means for the turbines placed in the upstream turbines' wake region, the spacing between these two turbines rows should be sufficiently large so that the tidal flow velocity could be significantly recovered. To this end, it is important to understand the wake structure downstream of turbine row.

3.5 Wake characteristics

The distribution of the peak tidal stream velocity over an ebb period with no turbine is showed in Figure 11(a) in which the red dotted rectangle is the turbine deployment area. Figure 11 shows the velocity distribution around the turbine deployment area. Figure 11(b) is the situation without turbine while Figures 11(c), (d) and (e) demonstrate the velocity distribution for turbines deployed in regular, staggered and optimized layout at the same time, respectively.

It is seen that there is no obvious difference of the velocity field for various situations at far field. Significant decrease of the tidal velocity, however, appears at the channel between Huoshashan Island and Reefs after the deployment of the turbine array. Slight increase of the tidal velocity is seen to occur at the channel between Smallhulu Island and Reefs when the turbine array is deployed. In the area just behind the turbine array and at the channel between Hulu Island and Putuoshan Island, there is no significant velocity difference for these three turbine layouts (the locations of various islands are shown in Figure 8). They all show a large deceleration area behind turbine array with locally acceleration at the two side of the wake area. The result is similar to the work by Chen et al. (2013).

To further investigate the effect of these three turbine array layouts, five points are selected, as shown in Figure 12, where velocity field is simulated for a full tide. In Figure 12, points 1, 2 and 3 are located at the center of the regular turbine array layout and are 10D, 20D and 30D behind the last row, respectively. Simulated velocity at these three locations is used to examine the effect of the distance away from the turbine array on the velocity field. Point 4 is at the channel between Huoshashan Island and Reefs, while the point 5 is at the channel between SmallHulu Island and Reefs. The velocity data at these two points demonstrate the impacts on the two channels due to the

deployment of the turbine array.

The simulation of this period begins at 5:30am 23 August 2013 and the simulated velocity field is shown in Figure 13. Figure 13(a) shows the simulated velocity at point 1 during a full tide. It is seen that all three turbine array layouts cause significant decrease of tidal stream velocity at 10D behind them. The largest velocity decrease appears at about 10:00am. For the regular layout and staggered layout at that time, tidal stream velocity decreases from 1.34m/s to 0.21m/s, namely an 84% decrease. As the actual flowing direction of tidal stream is not always perpendicular to the turbine array, the difference between the regular and staggered layout is negligible. Therefore, the deceleration of the tidal stream velocity caused by the regular and staggered layout is almost the same. As such, Fig. 13 shows that the lines represent the velocity profiles induced by the deployment of the regular and staggered turbine layouts overlap each other. For the optimized layout, tidal velocity decreases from 1.34m/s to 0.31m/s, namely a 76% decrease, which is smaller than other two layouts. This can be ascribed to the fact that the optimized turbine array layout is deployed closer to the center of the turbine deployment area, and thus the tidal stream has sufficient distance to recover before reaching the point 1. A smaller decline of tidal stream velocity can also be found after 13:30 pm when the tide begins to rise. The different layouts of turbine array lead to the same decline about 16%. The reason for this phenomenon is that the placement of the turbine array slows down the rising tide before the tide reaches the turbine array. Furthermore, it can be seen that the deceleration of the velocity varies with the initial velocity. The faster the initial velocity is, the greater deceleration takes place. However, various turbines layouts have no obvious impact on the tidal stream phase.

Figure 13(b) shows that the maximum velocity decrease is 92%, namely from 1.17m/s to

0.09m/s for the regular and staggered turbine array layouts, while for the optimized layout, the maximum deceleration is 85%. The reason is that in the far wake area, the tidal stream flowing through the turbines mixes well with the tidal stream flowing through the gap between turbines (such as the tidal stream flowing through point 1), leading to a greater decline than that for point 1. In terms of the tidal stream velocity during the flooding phase, it shows a slight decrease and the maximum decline is about 7%. Similar results are shown in Figure 13(c). However, one notable thing is that the difference between the influences caused by these three turbine array layouts becomes more negligible.

Figure 13(d) shows a great deceleration of the tidal stream velocity in the channel between Huoshashan Island and Reefs due to the deployment of turbines. Although this channel is far away from the turbine array, the maximum velocity at point 4 decreases from 1.57m/s to 1.00m/s, name about 36% decline. The velocity variation during the tidal period becomes flat. Differences caused by different turbine array layout are negligible.

Figure 13(e) shows that the deployment of the turbine array has insignificant effect on the tidal stream velocity in the channel between Smallhulu Island and Reefs, which is far away from the turbines. Peak velocity, however, appears slightly earlier during the ebb tide and decreases a little during the flooding phase.

4. Conclusion

In this paper, a two-dimensional numerical model is developed based on OpenTidalFarm. The measured data from the demonstrative project of tidal stream energy in Zhoushan Island are used to validate the numerical model. The validated model is then used to simulate the tidal steam around

Zhoushan Islands and to calculate the energy extractions by 18 turbines with three layouts. The wake characteristics of these three turbine array layouts are also studied.

The optimal layout for extracting tidal stream energy is the unstructured layout. In this layout, both the first row and second row of the turbines can extract energy from not decelerated tidal stream. The tidal stream velocity at the third row also recovers after a long distance away from second row of turbines as well as accelerated by the blockage effect induced by the second row.

For the two structured regular and staggered layouts, their energy extractions are almost the same, namely 6.15×10^4 kW·h for the regular layout and 6.24×10^4 kW·h for the staggered layout. This is partly because the direction of the tidal stream is not always perpendicular to the tidal turbines, which reduces the difference between the regular layout and staggered layout. In this study, the energy extraction from the optimized layout is much higher at 6.56×10^4 kW·h, which is about 5% higher than the energy outputs of those two structured layouts.

Five locations are selected to investigate the peak velocity variation in the wake area. Results show that the maximum deceleration in the wake of the turbine array not only takes place behind the last row of the turbine array, it may also occurs at locations (e.g. point 2) where the wake flow mixes completely. In the far area such as at point 4 and 5, the difference of the influence between these three layouts is insignificant. This means that the deployment of the turbine array can make a huge difference to the velocity distribution but there is no big difference for the velocity distribution variations caused by these three layouts.

This study shows that in the real ocean field, tidal stream turbines can be deployed in unstructured layout in order to achieve a high energy extraction efficiency. Therefore, it is important to deploy turbines in a way that the spacing between the adjacent rows is sufficiently large so that

the downstream turbines can benefit from the great tidal flow velocity recovery.

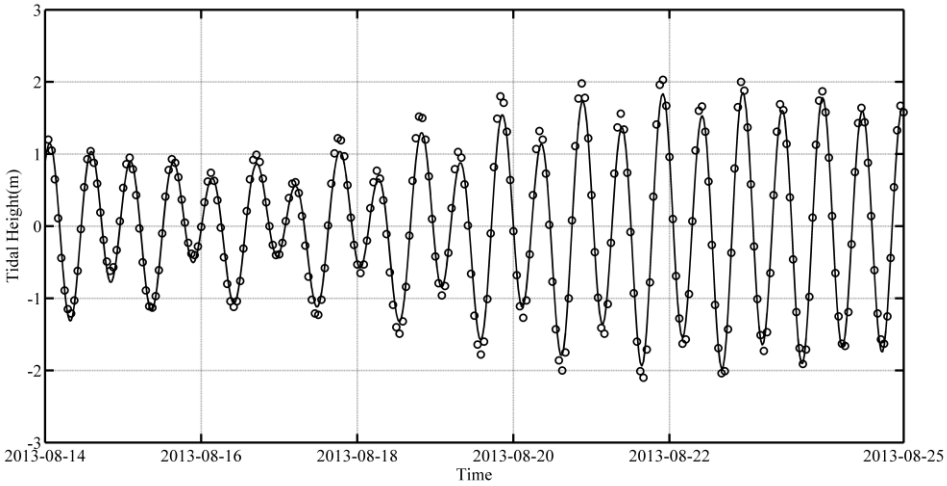

Figure 3. Comparisons between simulated and measured tidal heights at tidal height station B

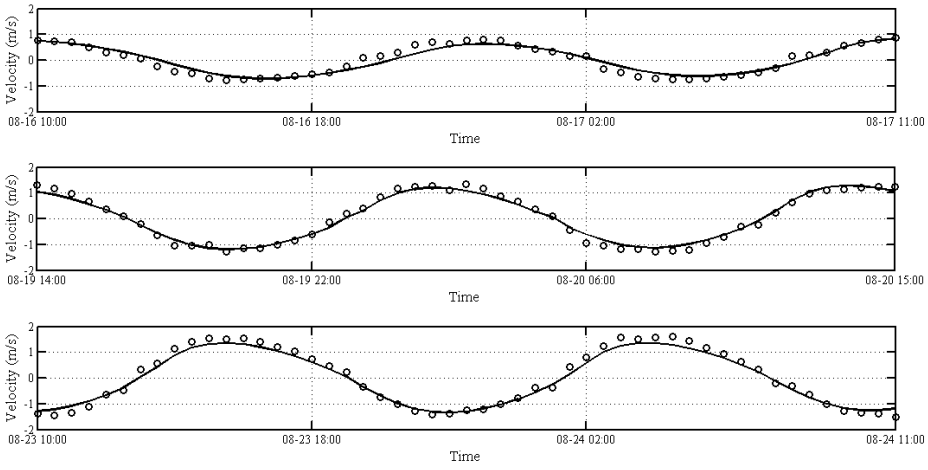

(a)

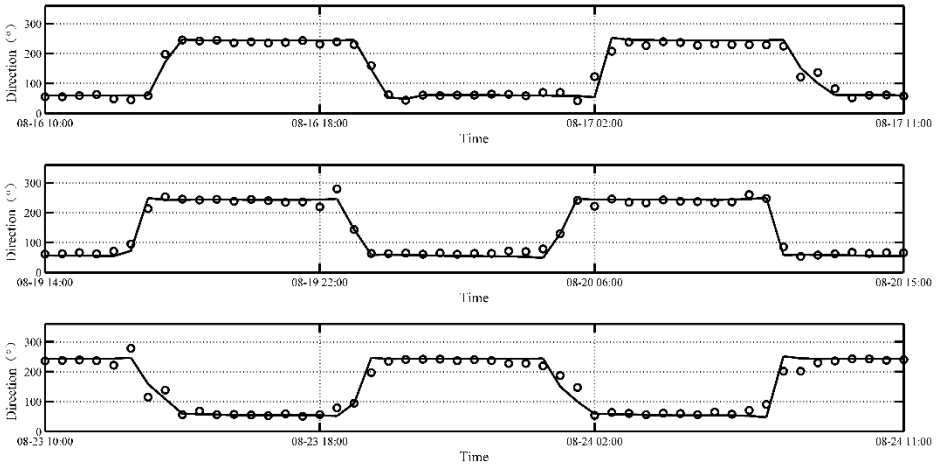

(b)

Figure 4. Comparisons between simulated and measured tidal stream velocity (a) and direction (b) at tidal monitoring station A5

Table 1. Statistical errors between the simulated and observed data.

Period	Types	MAE	RMSE
The neap tides (2013.8.16 10:00-2013.8.17 11:00)	Tidal height	0.08	0.10
	Tidal stream velocity	0.11	0.14
	Tidal stream direction	0.05	0.11
The middle tides (2013.8.19 14:00-2013.8.20 15:00)	Tidal height	0.17	0.19
	Tidal stream velocity	0.12	0.14
	Tidal stream direction	0.03	0.04
The spring tides (2013.8.23 10:00-2013.8.24 11:00)	Tidal height	0.10	0.12
	Tidal stream velocity	0.13	0.17
	Tidal stream direction	0.04	0.06
Total (2013.8.14 00:00-2013.8.25 00:00)	Tidal height	0.12	0.14
	Tidal stream velocity	0.12	0.15
	Tidal stream direction	0.04	0.07

Note: MAE: mean absolute error; RMSE: root mean square error.

Table 2. Detailed information about the four meshes

	Number of nodes	Number of cells
Mesh 1	130280	263747
Mesh 2	39002	79788
Mesh 3	7211	14937
Mesh 4	4310	8964

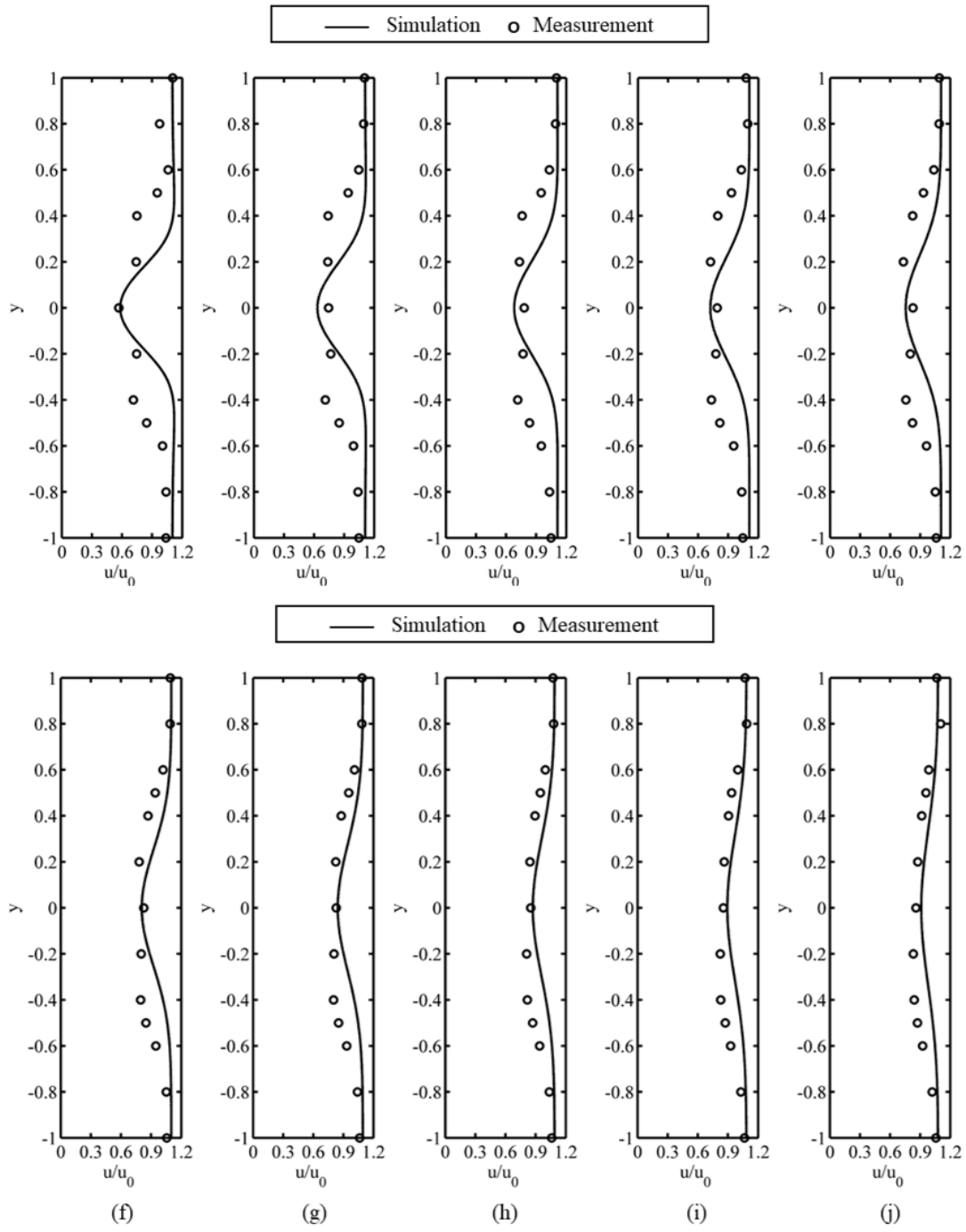

Figure. 5. Comparison of the wake velocities between the simulated data and measured data: (a) x/D = 1.0; (b) x/D = 1.5; (c) x/D = 2.0; (d) x/D = 2.5; (e) x/D = 3; (f) x/D = 4; (g) x/D = 5; (h) x/D = 6; (i) x/D = 7; (j) x/D = 8

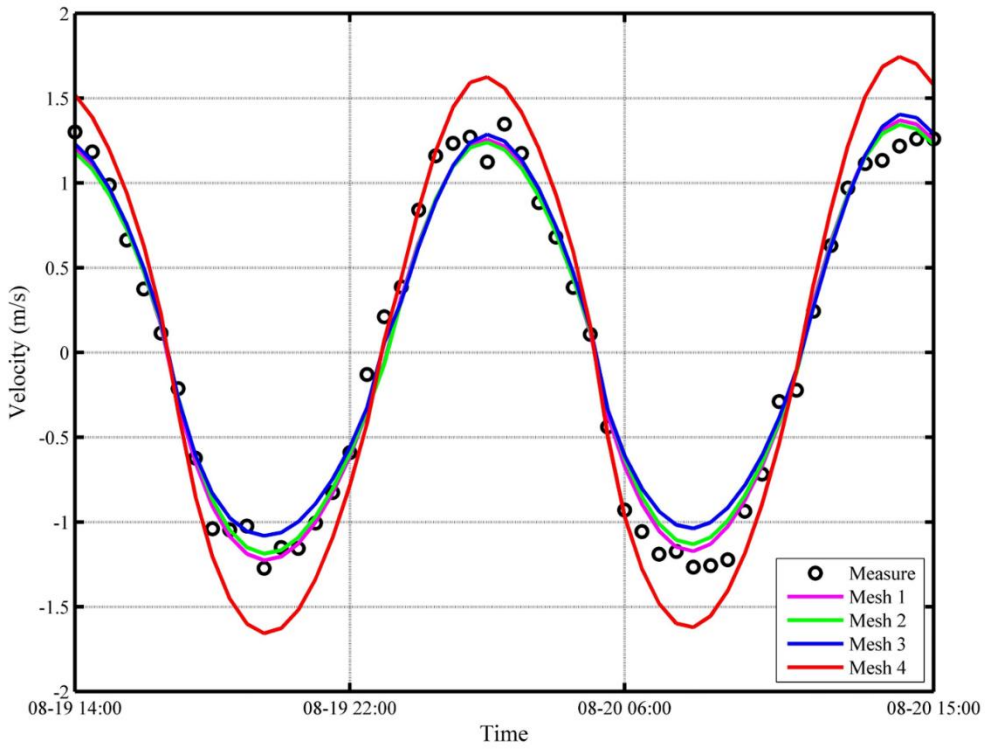

Figure 6. Sensitivity analysis of mesh size A5

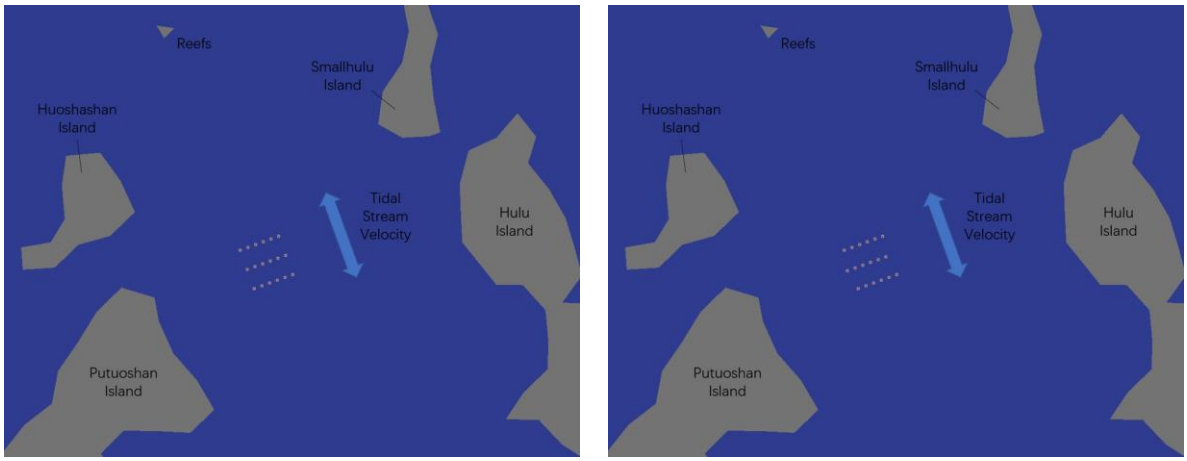

(a) (b)

Figure 7. The turbines (red dots) deployed in structured regular layout (a) and in structured staggered layout (b).

Figure 8. The turbines (red dots) deployed in unstructured optimized layout

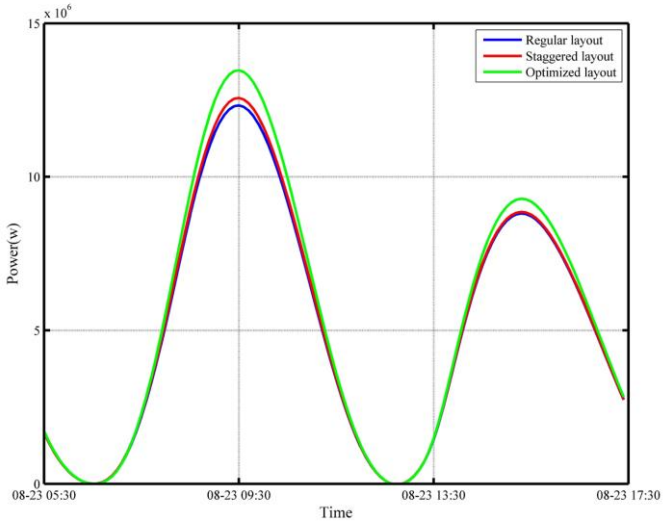

Figure 9. Power extraction of three layouts over 8 hours.

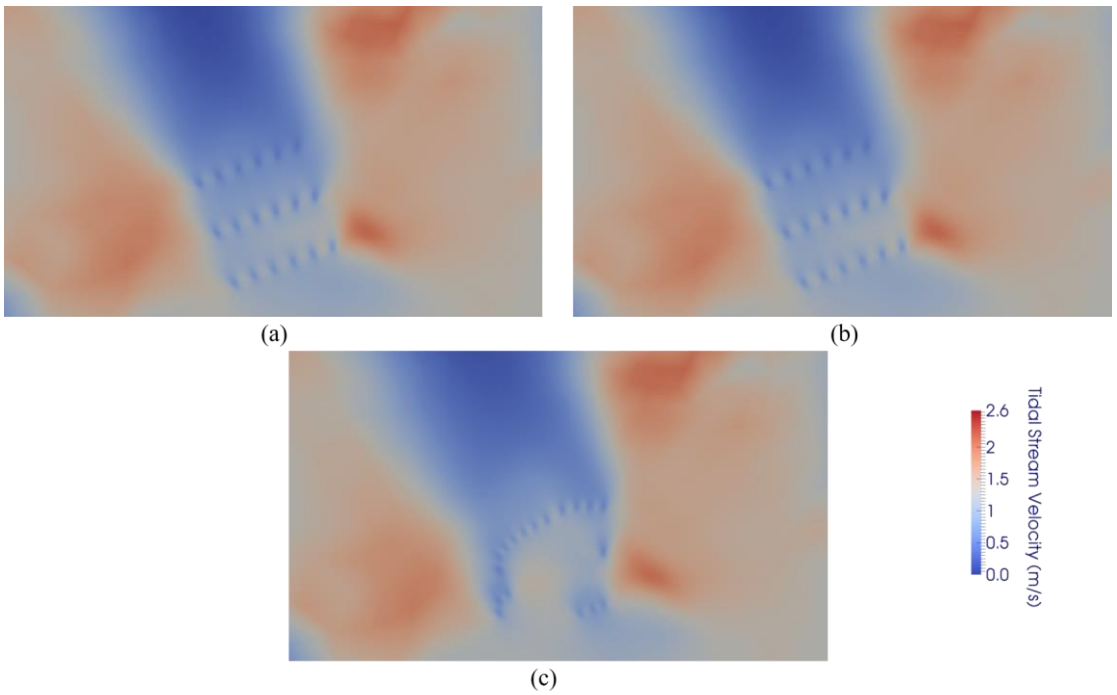

Figure 10. Distribution of the peak tidal stream velocity over a full ebb within the turbine area. (a) regular layout, (b) staggered layout (c) optimized layout

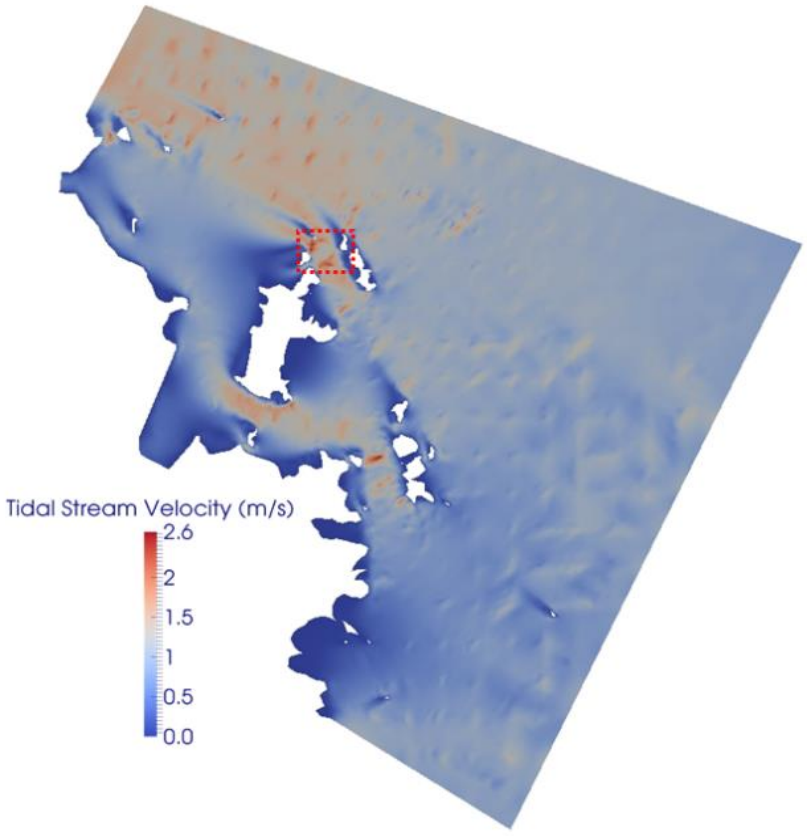

(a)

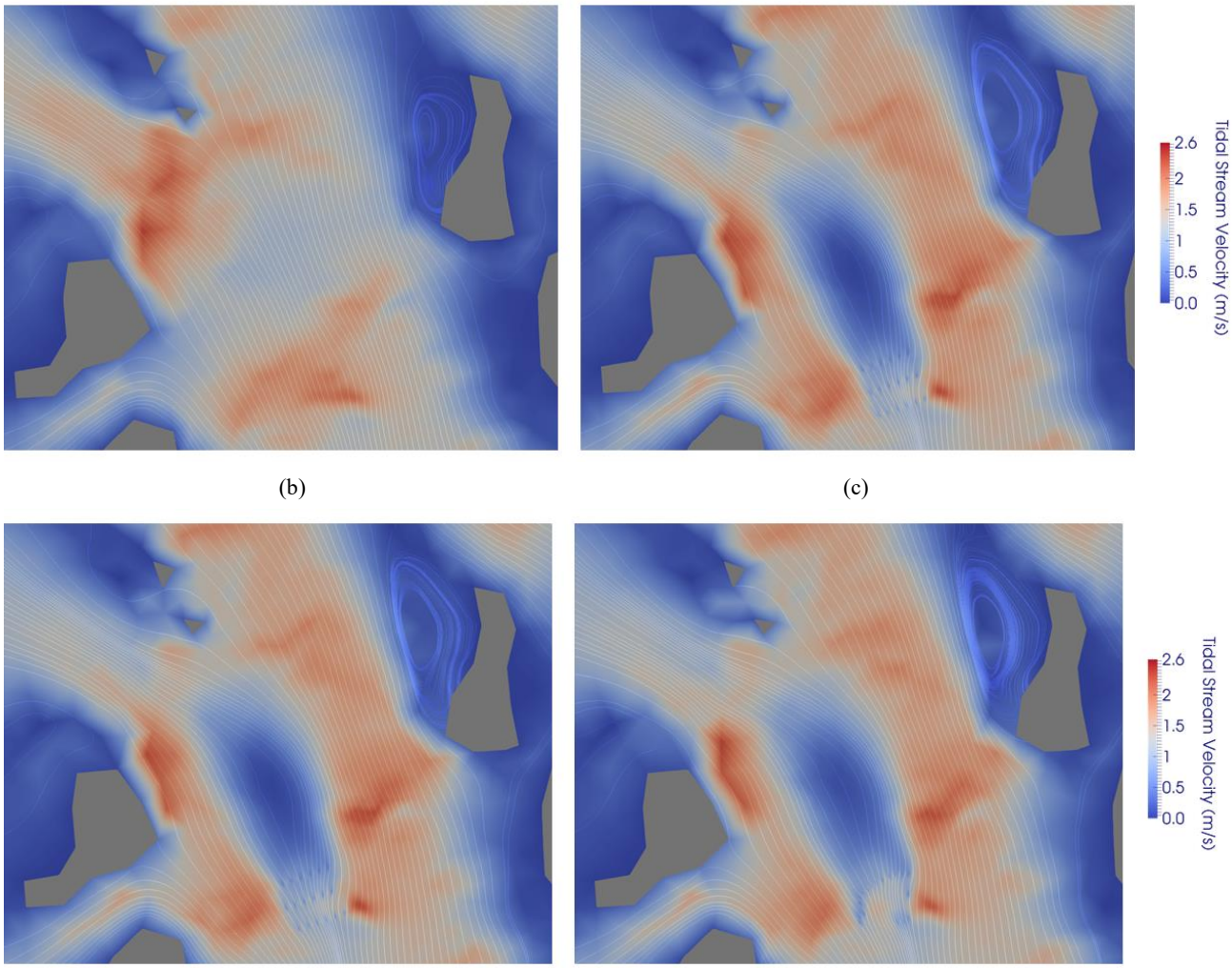

(b) (c)

(d) (e)

Figure 11. Distribution of the peak tidal stream velocity over a full ebb tide around Zhoushan Islands. (a) the distribution of velocities for the whole calculation area and the red rectangle is where the turbines would be deployed. (b) without turbine, (c) regular layout, (d) staggered layout (e) optimized layout

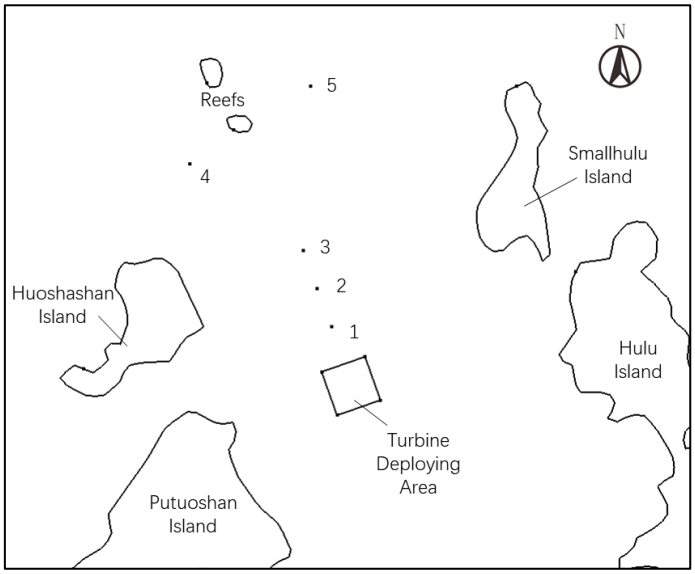

Figure 12. Positions of the five points where velocity field is simulated over a full tide. The square in the center is the area where turbines are developed.

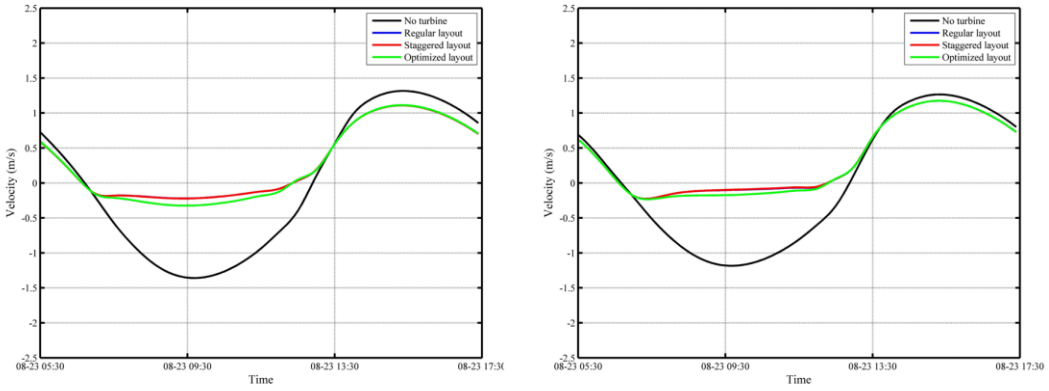

(a) (b)

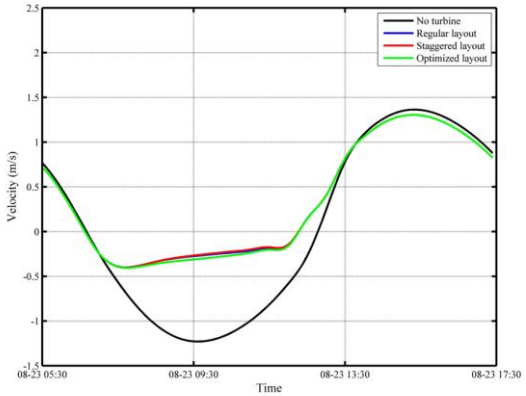

(c)

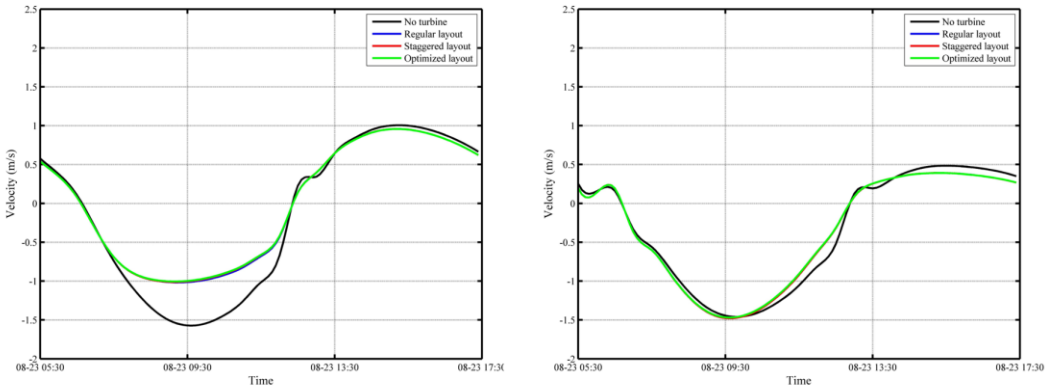

(e) (f)

Figure 13. Velocities change over a period including a full ebbtide at point 1 (a), point 2 (b), point 3 (c), point 4 (d), point 5(e).

Acknowledgments

The authors are grateful for sponsorship from the National Natural Science Foundation Council of China (51879098), and the Marine Renewable Energy Research Project of State Oceanic Administration (GHME2015GC01).

Reference:

References:

An B., 2012. Numerical Analysis of the Wake and Interaction Effect Analysis for tidal arrays in the Tidal Farm. Ocean University of China. Master thesis.

Boggs, P., Tolle J., 1995. Sequential Quadratic Programming *. Acta Numerica 4(4), 1-51

Chen Y., 2015. Study on the Effects of Tidal Turbine and Array on the Flow Field. Tsinghua University. Ph.D. thesis.

Chen, W., Liu W., Hsu M., 2013. Modeling Evaluation of Tidal Stream Energy and the Impacts of Energy Extraction on Hydrodynamics in the Taiwan Strait. Energies 6(4), 2191-2203.

Culley D., Funke S., Kramer S., Piggott M., 2016. Integration of cost modelling within the micro-siting design optimisation of tidal turbine arrays. Renewable Energy 85, 215-227.

Culley D., Funke S., Kramer S., Piggott M., 2017. A surrogate-model assisted approach for optimising the size of tidal turbine arrays. International Journal of Marine Energy 19, 357-373.

Divett T., Vennell R., Stevens C., 2013. Optimization of multiple turbine arrays in a channel with tidally reversing flow by numerical modelling with adaptive mesh. Philos Trans A Math Phys Eng Sci 371 (1985), 20120251.

Evans, G.P., 1993. A framework for marine and estuarine model specification in the UK. Water Research Centre, pp. 64. Marlow, UK.

Feu R., Funke S., Kramer S., Culley D., Hill J., Halpern B., Piggott M., 2017. The trade-off between tidal-turbine array yield and impact on flow: A multi-objective optimisation problem. Renewable Energy 114, 1247-1257.

Funke S., Farrell P., Piggott M., 2014. Tidal turbine array optimisation using the adjoint approach. Renewable Energy 63, 658-673.

Funke S., Kramer S., Piggott M., 2016. Design optimisation and resource assessment for tidal-stream renewable energy farms using a new continuous turbine approach. Renewable Energy 99, 1046-1061.

Garrett, C., Cummins, P., 2008. Limits to tidal current power 33 (11), 2485-2490.

González-Gorbeña, E., Qassim R., Rosman P., 2016. Optimisation of hydrokinetic turbine array layouts via surrogate modelling. Renewable Energy 93(8), 45-57.

González-Gorbeña, E., Qassim R., Rosman P., 2018. Multi-dimensional optimisation of Tidal Energy Converters array layouts considering geometric, economic and environmental constraints. Renewable Energy 116, 647-658.

Guo, Y.K., Wu, X.G., Pan, C.H. and Zhang, J.S., 2012. Numerical Simulation of the Tidal Flow and Suspended Sediment Transport in the Qiantang Estuary, ASCE Journal of Waterway, Port, Coastal and Ocean Engineering, 138: 192-203.

Guo, YK, Zhang, ZY and Shi, B. 2014. Numerical simulation of gravity current descending a slope into a linearly stratified environment. Journal of Hydraulic Engineering (ASCE), 140(12) DOI: 10.1061/(ASCE)HY.1943-7900.0000936.

Lin, Z., Pokrajac, D., Guo, Y.K., Jeng, D.-S., Tang, T., Rey, N., Zheng, J., Zhang, J. 2017. Investigation of nonlinear wave-induced seabed response around mono-pile foundation. Coastal Engineering, 121: 197-211

Malki, R., Williams, A., Croft, T., Togneri, M., Masters, I., 2013. A coupled blade element momentum – Computational fluid dynamics model for evaluating tidal stream turbine

performance. Applied Mathematical Modelling 37 (5), 3006-3020.

Mycek P., Gaurier B., Germain G., Pinon G., Rivoalen E., 2012. Numerical and experimental study of the interaction between two marine current turbines. In: In: European Wave and Tidal Energy Conference 2011, Southampton : United Kingdom (2011).

O'Doherty D., Mason- Jones A., Morris C., O'Doherty T., Byrne C., Prickett P., Grosvenor R., 2011. Interaction of marine turbines in close proximity. In: In: European Wave and Tidal Energy Conference.

OpenTidalFarm, 2014. https://opentidalfarm.readthedocs.io/en/latest/.

Sutherland, G., Foreman M., Garrett C., 2007. Tidal current energy assessment for Johnstone Strait, Vancouver Island. Proceedings of the Institution of Mechanical Engineers, Part A: Journal of Power and Energy 30(2), 175-177.

Vennell R., 2010. Tuning turbines in a tidal channel. Journal of Fluid Mechanics 663(11), 253-267.

Vennell R., 2011. Tuning tidal turbines in-concert to maximise farm efficiency. Journal of Fluid Mechanics 671(3) 587-604.

Vennell R., Funke S., Draper S., Stevens C., Divett T., 2015. Designing large arrays of tidal turbines: A synthesis and review. Renewable and Sustainable Energy Reviews 41, 454-472.

Vennell, R., 2012. The energetics of large tidal turbine arrays. Renewable Energy 48, 210-219.

Wang Y., 2018. Research on Resource Assessment of Tidal Stream Energy and Layout Optimization of Turbine Array. Hohai University. Master thesis.

Wang Z., Zhou L., Zhang G., Wang A., 2010. Tidal Stream Energy Assessment in Specific Channels of Zhoushan Sea Area. Periodical of Ocean University of China 40(8), 27-33.

Xin X., Shao X., Deng J., Li W., 2011. Hydrodynamic performance prediction of marine current

turbine with dual rotor in tandem arrangement. Journal of Zhejiang University (Engineering Science) 45(7), 1227-1231.

Zhang, J.S., Lin, X., Wang, R., Guo, Y.K., Zhang, C., Zhang, Y., 2020. Flow structures in wake of a pile-supported horizontal axis tidal stream turbine. Renewable Energy 147, 2321-2334.

Zhang J., Cao Y., Wu X., Song F., Dai P., 2017. Investigation of hydrodynamic characteristics around parallel-arranged horizontal-axis tidal stream turbines. Journal of Hohai University (Natural Sciences) 45(3), 256-262.

Zhang J., Wang Y., Tang Z., Fan W., Zhang T., 2018. Site selection and layout optimization of turbines in the Demonstration Project of Zhoushan Tidal Stream Energy. Journal of Hohai University (Natural Sciences) 46(3), 240-245.

Zhang J.S., Wang, R., Guo, Y.K., Wu, X., Zheng, J.H., Zhang, Z., 2019. Modelling study of hydrodynamics in a macro tidal estuary. ICE Maritime Engineering, 172(2), 34-44.

Zhang L., Li X., Geng J., Zhang X., 2013. Tidal current energy update 2013. Advances in New and Renewable Energy 1(1), 53-68.